In-beam γ-ray spectroscopy of ^{68}Fe from charge exchange on ^{68}Co projectiles

A. Gade ,[1,2] R. V. F. Janssens ,[3] B. A. Brown,[1,2] R. G. T. Zegers,[1,2] D. Bazin ,[1,2] P. Farris,[1,2] A. M. Hill ,[1,2] J. Li,[1]
D. Little,[3] B. Longfellow,[1,2,*] F. Nowacki,[4,5] D. Rhodes,[1,2] and D. Weisshaar [1]

[1]*National Superconducting Cyclotron Laboratory, Michigan State University, East Lansing, Michigan 48824, USA*
[2]*Department of Physics and Astronomy, Michigan State University, East Lansing, Michigan 48824, USA*
[3]*Department of Physics and Astronomy, University of North Carolina at Chapel Hill, Chapel Hill, North Carolina 27599, USA*
and Triangle Universities Nuclear Laboratory, Duke University, Durham, North Carolina 27708, USA
[4]*Universitè de Strasbourg, IPHC, 23 rue du Loess 67037 Strasbourg, France*
[5]*CNRS, UMR7178, 67037 Strasbourg, France*

Excited states in the neutron-rich nucleus ^{68}Fe were populated using a ^{9}Be(^{68}Co, ^{68}Fe + γ)X charge-exchange reaction at 95 MeV/u. The new γ-ray transitions reported here for the first time complement data from β-decay studies and nucleon knockout reactions. In comparison to shell-model calculations with the LNPS effective interaction, two candidate states for the 6_1^+ level emerge. The distinct population pattern of excited states and the magnitude of the cross section, $\sigma_{\mathrm{inc}} = 0.51(6)$ mb, make this reaction a promising one for future in-beam γ-ray spectroscopy. Reaction calculations with nuclear structure input from a new, locally optimized Hamiltonian, $f7j4a$, together with general considerations for heavy-ion-induced charge-exchange reactions appear consistent with most of the observations, although challenges remain.

I. INTRODUCTION

The properties of neutron-rich nuclei and, in particular, the modifications to their structure when compared to that of systems closer to the valley of stability have been fueling rare-isotope research at accelerator facilities around the world. With the ultimate goal of achieving a predictive model for nuclei across the nuclear chart, the properties of rare isotopes in regions of rapid structural change represent demanding benchmarks with the potential to improve models through experiment-theory confrontations.

The Cr, Fe, and Ni isotopes around neutron number $N = 40$, and towards $N = 50$, are such examples [1,2]. Beyond the valley of β stability, the energy of the first excited 2^+ state in even-even nuclei is often among the first accessible experimental observables, providing a valuable indicator of the intrinsic shell structure. This is illustrated in Fig. 1, which depicts the evolution of the $E(2_1^+)$ excitation energy along the Cr, Fe, and Ni isotopic chains from the proton dripline to the last isotope where this quantity is known. The proton-magic ($Z = 28$) Ni isotopes display high $E(2_1^+)$ energies at the $N = 28$ and 50 magic numbers, as well as at $N = 40$, where the parity change between the fp shell and the $g_{9/2}$ orbital limits possible neutron configurations for the 2_1^+ state to configurations of 2-particle 2-hole (2p-2h) character [3]. A stunning change is visible in Fig. 1 for the Fe and Cr isotopic chains with just two and four fewer protons than Ni, respectively. While they exhibit an elevated 2_1^+ energy at $N = 28$,

collectivity appears to develop rapidly towards $N = 40$, as indicated by some of the smallest $E(2_1^+)$ values in the region. In the Fe isotopes, the minimum in $E(2_1^+)$ energy and, thus, the maximum collectivity occurs for ^{70}Fe ($N = 44$) as the 2_1^+ energy in ^{72}Fe has been established to increase on the path towards $N = 50$ [4]. In the Cr isotopic chain, the 2_1^+ energy is known to decrease at least out to $N = 42$, ^{66}Cr, the last studied $Z = 24$ isotope where spectroscopic information is presently available [4]. Large-scale shell-model calculations with the LNPS (Lenzi-Nowacki-Poves-Sieja) effective interaction [2] in the full fp shell for protons and the $f_{5/2}$, $p_{3/2}$, $p_{1/2}$, $g_{9/2}$, and $d_{5/2}$ orbitals for neutrons have confirmed the picture described above. In this work, the LNPS interaction is used with recent small adjustments [2,5–7] to extend its reliability up to neutron number $N = 50$, including $g_{9/2}$-$d_{5/2}$ particle-hole excitations, with minor consequences at $N = 40$.

Recently, in this very neutron-rich region, first information on the excited states beyond the 2_1^+ level has been obtained with one-proton removal reactions that, with large cross sections, selectively populate states associated with strong single-hole configurations relative to the projectile ground state (see, e.g., Refs. [4,7–10]) for ^{70,72}Fe, ^{66}Cr, ^{78}Ni, and ^{60,62}Ti. Also selective β-decay studies have reached beyond the first 2^+ state for ^{68,70}Fe and ^{64}Cr [11–13].

The present work focuses on a novel approach to reach excited states in ^{68}Fe. The spectroscopy of excited states in this nucleus has only recently become possible. Discovered among the projectile fragmentation residues of ^{86}Kr in the 1980s [15], and observed to be formed in the neutron-induced fission of ^{239}Pu in the 1990s [16], excited states, assigned 2_1^+ and (4_1^+), were first reported from in-beam γ-ray spectroscopy with knockout reactions in 2008 [17] and,

subsequently, following the β decay of ^{68}Mn [11,12,18], where additional low-spin states were established. While the determination of the low 2_1^+ energy of 522 keV in ^{68}Fe signaled the persistence of collectivity in the Fe isotopic chain beyond $N = 40$, as already conjectured by Hannawald *et al.* [19], intermediate-energy Coulomb excitation ultimately quantified the quadrupole collectivity from a measurement of the $B(E2 \uparrow)$ excitation strength [20]. Recently, the masses of nuclei in the region around ^{68}Fe were measured via the time-of-flight technique [21,22], and these garnered attention in view of their importance for modeling neutron-star crust cooling.

Here, the inverse-kinematics γ-ray-tagged, charge-exchange reaction, ^{9}Be(^{68}Co, ^{68}Fe + γ), is used at 95 MeV/u to produce ^{68}Fe in excited states complementing those reported earlier from nucleon removal reactions and β decay. Such ^{9}Be-induced nucleon-exchange reactions leading to residues more exotic than the projectile were pioneered for γ-ray spectroscopy in the first study of ^{46}S [23]. These have since also been used on the neutron-deficient side of the valley of stability to produce excited levels up to 8^+ in ^{78,76}Sr for the determination of excited-state lifetimes [24].

The ^{68}Co projectile is suggested to exhibit two β-decaying states; one with negative parity and high spin was given a tentative (7^-) assignment in Ref. [25] and was proposed to be the ground state. The other is then purported to be a low-spin, positive-parity isomer, originally suggested to have spin-parity (3^+) [25], but more recently given a tentative (1^+) assignment [26]. A recent Penning-trap mass measurement [27] provided evidence that mostly the high-spin, long-lived state was populated in ^{68}Co ions produced by ^{76}Ge projectile fragmentation. In a single-particle picture, the charge exchange from the proposed 7^- ^{68}Co ground state can produce, for example, $J = 6^+$ levels in ^{68}Fe via the exchange of a $f_{7/2}$ proton and a $g_{9/2}$ neutron. Other medium-spin states could be reached as well. More detailed estimates of the charge-exchange cross section are presented in the discussion section below.

II. EXPERIMENT

The measurement was performed at the National Superconducting Cyclotron Laboratory's (NSCL) Coupled Cyclotron Facility [28]. The secondary beam containing the ^{68}Co projectiles was produced by fragmentation of a 140-MeV/u ^{82}Se stable beam impinging on a 329-mg/cm^2 ^{9}Be production target and was separated with a 300-mg/cm^2 Al degrader in the A1900 fragment separator [29]. The separator's momentum acceptance was restricted to $\Delta p/p = 2\%$. The secondary beam cocktail contained 46% of ^{68}Co, 40% of ^{66}Fe, and 9.5% of ^{65}Mn as its most intense components. The 376-mg/cm^2-thick ^{9}Be reaction target was located at the target position of the S800 spectrograph. Projectilelike reaction residues were identified on an event-by-event basis in the S800 focal plane [30] from their energy loss and flight time.

For the first half of the experiment, the magnetic rigidity of the spectrograph was optimized to center ^{64}Cr products from ^{65}Mn projectiles in the focal plane, while the second half proceeded with the magnetic rigidity slightly shifted
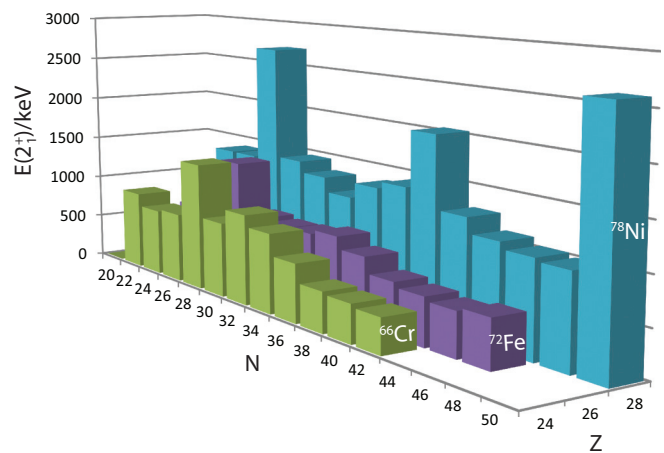

FIG. 1. Evolution of 2_1^+ energies [4,7–9,14] in the Cr, Fe, and Ni isotopic chains from the proton dripline to the last known neutron-rich isotope for each species.

to move ^{64,62}Cr ejectiles from ^{66}Fe and ^{68}Co beams more into the focal-plane acceptance—the spectroscopy of these two neutron-rich Cr isotopes was the original focus of the measurements, and results have been published recently [31]. Coincidentally, the first setting above also centered ^{68}Fe ions from reactions with the ^{68}Co secondary beam in the spectrograph. The particle identification for ^{68}Fe is illustrated in Fig. 2. For this spectrum, the ^{68}Co projectiles in the entrance channel were selected through a software gate applied on the time-of-flight difference taken between two plastic timing scintillators located upstream of the target. Because ^{66}Fe and ^{68}Co projectiles were essentially equally intense and overlapped in the time-of-flight difference, they could not be separated in the incoming beam at the $\Delta p/p = 2\%$ momentum acceptance. As a result, the corresponding particle identification spectrum contains reaction products originating from both of these incoming species. However, since fast-beam, two-neutron pickup reactions onto neutron-rich nuclei are expected to proceed with negligible cross sections, ^{68}Fe production in this setting is most probably exclusively from charge exchange on ^{68}Co projectiles. Figure 2(a) shows the particle identification based on energy loss vs time-of-flight.

The ^{68}Fe longitudinal momentum distribution is presented in Fig. 2(b). The range displayed in this spectrum corresponds to the full S800 acceptance, herewith confirming that this reaction channel was, indeed, essentially centered and not subject to acceptance cuts. The distribution is only marginally broadened with respect to the 2%-wide incoming-beam momentum profile, in agreement with the observations reported in Ref. [23]. The inclusive cross section for ^{68}Co-to-^{68}Fe charge exchange was determined from the number of ^{68}Fe products detected in the S800 focal plane relative to the number of ^{68}Co projectiles taking the number density of the target into account. Since the experiment was optimized for γ-ray spectroscopy only, and the incoming beam was not closely monitored for possible, time-dependent changes in composition, only a few hours of data in between the first nor-
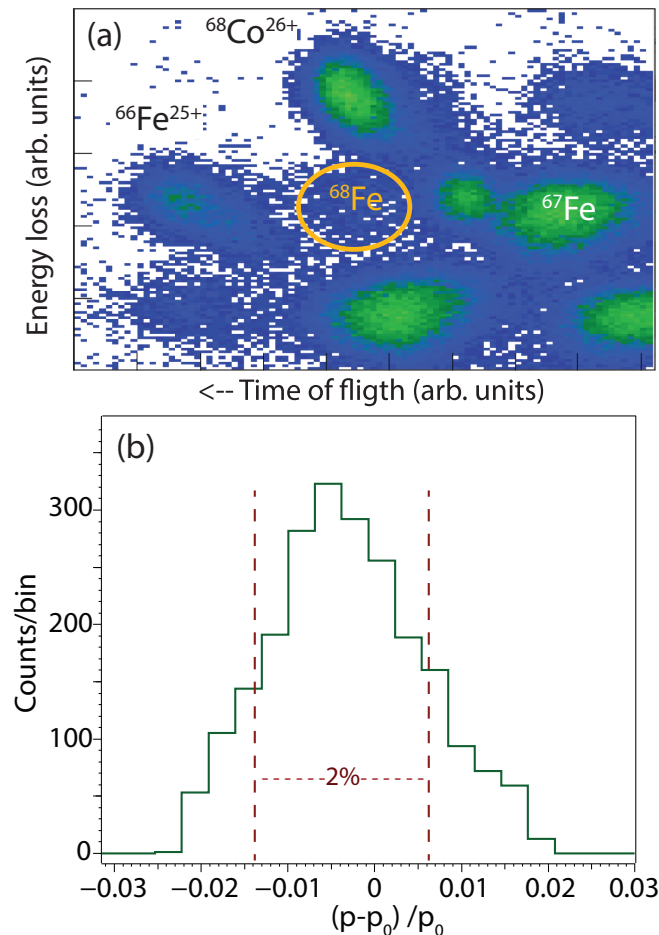
FIG. 2. (a) Particle identification of Fe isotopes produced from ^{68}Co projectiles. The ^{68}Co ions in the secondary beam could not be separated from the ^{66}Fe ones via a time-of-flight difference cut. However, the reaction residues shown have more neutrons than ^{66}Fe and have been produced from ^{68}Co (see text for further details). The hydrogenlike charge states of ^{66}Fe and ^{68}Co are visible. ^{68}Fe ions produced from ^{68}Co and the ^{68}Co^{26+} charge state have the same A/Q ratio and, thus, have the same flight time as visible. (b) Longitudinal momentum distribution of ^{68}Fe ions with $p_0 = 27.0$ GeV/c. The full S800 acceptance is shown, and the 2% momentum width of the incoming beam is indicated.

malization run and a cyclotron retune were used to determine an inclusive cross-section value of $\sigma_{inc} = 0.51(6)$ mb.

The high-resolution GRETINA γ-ray array [32,33] of 36-fold segmented high-purity germanium detectors, grouped into modules of four crystals each, surrounded the reaction target and detected prompt γ radiation emitted in flight by the reaction products. The 11 GRETINA modules available at the time of the experiment were arranged in two rings with 4 modules located at 58° and the other 7 modules at 90° with respect to the beam axis. One of the 16 crystals at forward angles was turned off due to a technical problem. Online pulse-shape analysis determined the photon interaction points required for event-by-event Doppler reconstruction of the γ rays emitted in-flight at a recoil velocity of about $v/c = 0.4$. The hit with the maximum energy deposition was chosen as
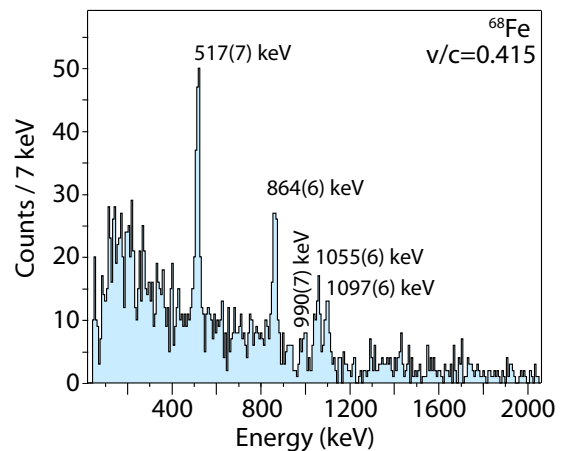

FIG. 3. Doppler-corrected energy spectrum with addback for ^{68}Fe products from charge exchange with ^{68}Co projectiles. The peaks at 517 and 864 keV correspond to the known γ-ray transitions depopulating the 2_1^+ and (4_1^+) states, respectively. The other peaks are new transitions in ^{68}Fe reported here for the first time.

the first interaction point for the computation of the γ-ray emission angle entering the Doppler reconstruction [33]. The trajectory of projectilelike reaction residues, as ray-traced through the S800 spectrograph, was incorporated into the emission-angle determination as well. Figure 3 displays the Doppler-reconstructed γ-ray spectrum for ^{68}Fe, with nearest-neighbor addback included [33].

III. RESULTS AND DISCUSSION

The four dominant peaks in the ^{68}Fe spectrum of Fig. 3 correspond to the two known γ-ray transitions, $2_1^+ \rightarrow 0_1^+$ and $(4_1^+) \rightarrow 2_1^+$, and to two new ones at 1055(6) and 1097(6) keV, respectively. A fifth, weaker peak at 990(7) keV is more prominent in the coincidence analysis below. The energies reported for the two known transitions agree within uncertainties with previous data [14]. The absolute γ-ray intensities, obtained from the peak areas corrected for the simulated GRETINA efficiencies, and including the effects of the Lorentz boost, readily reveal an interesting scenario: the $2_1^+ \rightarrow 0_1^+$ and $(4_1^+) \rightarrow 2_1^+$ transitions exhaust 41(6)% and 40(6)% of the total number of ^{68}Fe recoils detected. Since these two transitions are coincident, this observation implies (i) that the population of the 2_1^+ state is, within errors, due to feeding from the (4_1^+) level and (ii) that there is little room for additional transitions feeding directly into the 2_1^+ level. With this in mind, the strong transitions observed above 1 MeV must then originate from levels located above the (4_1^+) state in the level scheme, likely with J^π quantum numbers preventing strong direct decay to the 2_1^+ level. As shown below, direct decay of the transitions to the ground state is ruled out by the observed coincidence relationships. In addition, should the 1055- and 1097-keV γ rays feed the (4_1^+) state in parallel, their sum would exhaust 94(13)% of the intensity recorded for the decay out of this level (see Table I). These observations motivate the coincidence analysis presented below despite the low available statistics.

TABLE I. Relative intensities I_γ of the γ-ray tran-
sitions with energy E_γ extracted from the γ-ray singles
spectrum. We note that these were determined from a
spectrum without addback because then the detection
efficiency is well understood [33].

E_γ (keV)	I_γ (%)
517	100(14)
864	100(14)
990	21(8)
1055	51(9)
1097	43(10)

Surprisingly, the coincidence analysis reveals the presence
of several additional transitions not clearly visible in the sin-
gles spectrum. Figures 4 and 5 provide the projection of the
$\gamma\gamma$-coincidence matrix (top) followed by coincidence spectra
[panels (b) to (f) and panels (b) to (d), respectively] with the
specific gate conditions indicated in the figures. The projec-
tion clearly amplifies the γ-ray transition at 990 keV and those
around 1 MeV, as well as a peak structure at 827 keV just
below the $(4_1^+) \rightarrow 2_1^+$ transition and, possibly, three additional
peaks at 400, 624, and 752 keV. These are labeled in Fig. 5
with their energy and associated uncertainties. This figure
shows coincidence spectra from sums of gates or gates placed
on a broad spectral region, herewith increasing statistics in
comparison to Fig. 4. While the observations are not sufficient
to build a level scheme, due to marginal statistics, it is never-
theless clear that the three γ rays between 900 and 1100 keV
are in (weak) coincidence with the 517- and 864-keV transi-
tions. Figure 5(b) also strengthens the case for the presence
of a weak 827-keV transition that becomes clear only from
the projection and coincidence spectra. There is also some
evidence for several additional weak transitions located higher
up in the level scheme, at least above the (4_1^+) state (400
and 624 keV) and possibly above the 1097-keV transition
(752 keV). An excess of counts between 1.2 and 2 MeV
returns coincidence events with the $(4_1^+) \rightarrow 2_1^+$ transition and
with the trio of peaks between 900 and 1100 keV. As pointed
out above, the direct cross section to the ground state in the
present reaction amounts to 59(9)%, a value obtained from
the inclusive cross section by subtraction of all direct feeders
to the ground state. In this case, following the coincidence
analysis and the intensity arguments above, this feeding ap-
pears to be from the 2_1^+ level only. Hence, the charge exchange
induced by the ^{68}Co projectile appears to populate the ground
state of ^{68}Fe directly as well as high-lying, higher-spin states
that then cascade through the (4_1^+) and 2_1^+ levels toward the
ground state. This observation is, perhaps, plausible given
the possibility that both the high-spin ground state and the
low-spin isomer could be present in the ^{68}Co projectile beam.
However, it should be noted that, for example, the population
of high-lying 1^+ states with strong decays toward the ground
state is likely missed under the present experimental condi-
tions of low γ-ray statistics. This unobserved feeding could
inflate the reported ground-state cross section.

Figure 6 compares the emerging picture of the proposed
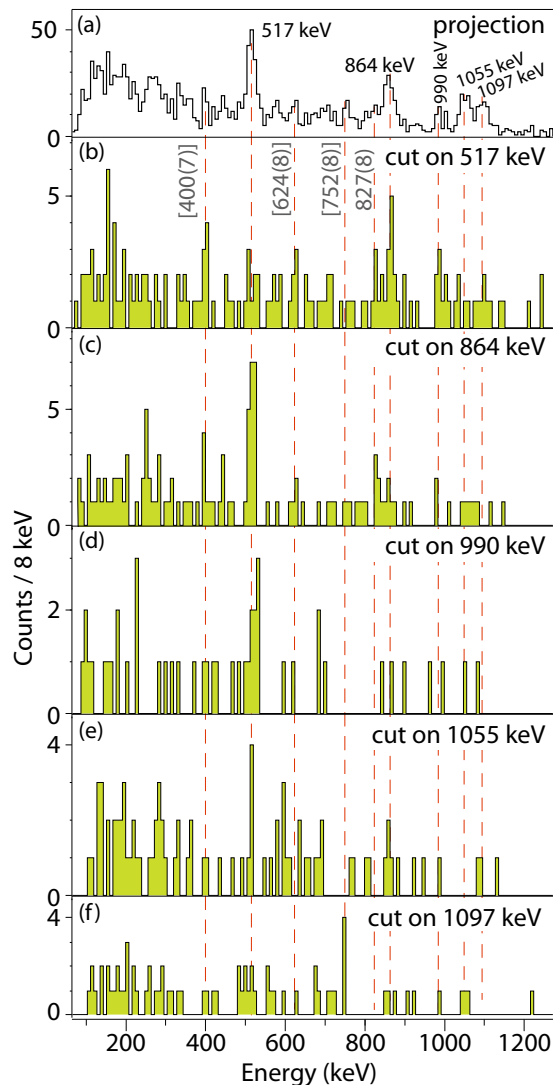^{68}Fe level scheme with predictions for the yrast cascade as

FIG. 4. Projection of the $\gamma\gamma$-coincidence matrix (a) and coin-
cidence spectra obtained from cuts placed on the labeled γ-ray
transitions, panels (b) to (f). From the counts in the 1055- and 1097-
keV peaks in the addback singles spectrum and the corresponding
GRETINA detection efficiency, one expects 4 and 3 counts in the
864-keV peak in panels (e) and (f), respectively, and 5(2) and 3(2)
counts are observed.

calculated with the LNPS effective interaction (left) and with
a new, "locally optimized" Hamiltonian (right), used below
to generate input for reaction theory calculations. The cor-
responding, relatively simple, model space consists of the
$0f_{7/2}$ orbital for protons and the $0f_{5/2}$, $1p_{3/2}$, $1p_{1/2}$, and
$0g_{9/2}$ orbitals (notated by $j4$) for neutrons. This model space
postulates that ^{48}Ca, ^{56}Ni, and ^{78}Ni have closed-shell config-
urations, and it is referred to as $f7j4$ below. The Hamiltonian
uses the neutron-neutron Hamiltonian from Ref. [34] that is
constrained to fit the binding energies (relative to ^{56}Ni) and
the low-lying spectra of the Ni isotopes. The proton-proton
Hamiltonian is taken from the energy spectrum of $J = 0, 2, 4,$
and 6 levels in ^{54}Fe, and the proton-neutron part is based on
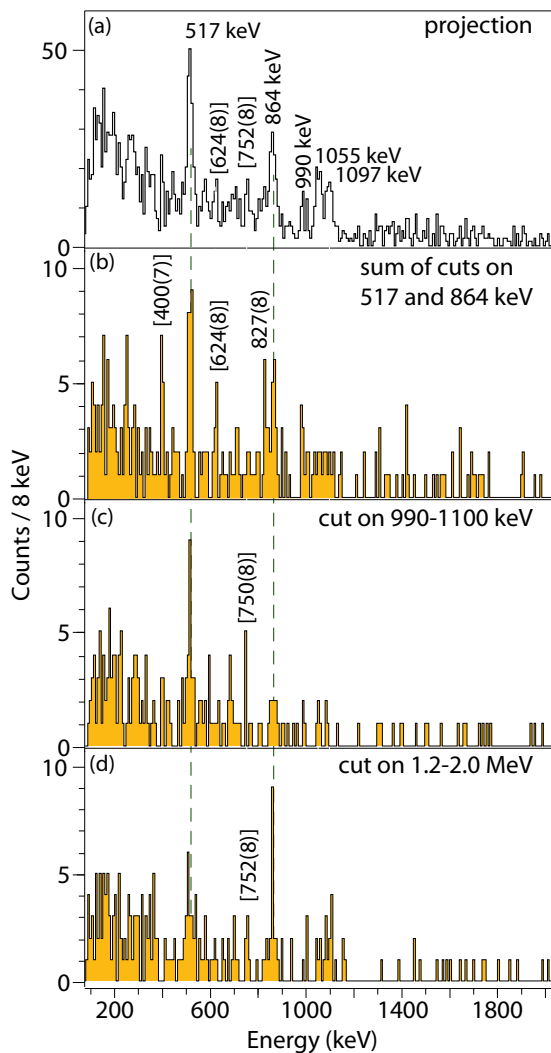the renormalized nucleon-nucleon interaction from Ref. [35].

FIG. 5. Projection of the $\gamma\gamma$-coincidence matrix (a) and coincidence spectra obtained from cuts on the labeled γ-ray transitions or energy regions, panels (b) to (d). The proposed new transition at 827 keV, albeit hardly visible in the projection, becomes prominent in the sum spectrum coincident with the yrast cascade and, thus, is most probably located above the (4_1^+) state in the level scheme. There is weaker evidence for the other proposed transitions and their energy labels are placed in brackets, accordingly.

The calculations with this $f7j4$ Hamiltonian are not at a level of precision comparable to those with the LNPS interaction, but they illustrate (i) the complexity of the low-lying level scheme, which appears to be largely bypassed by the reaction mechanism used here; (ii) the density of medium-spin states expected to be populated in charge exchange from a 7^- state; and (iii) the expected onset of negative-parity states already at 2.4 MeV, which should add to the complexity of the level scheme. In the following, the nuclear structure input from this computationally easy-to-use Hamiltonian is used to explore the population of final states in the charge-exchange reaction leading to ^{68}Fe.

While it is not possible to calculate accurately the cross section for the ^{68}Co(^{9}Be, ^{9}B)^{68}Fe* reaction without proper
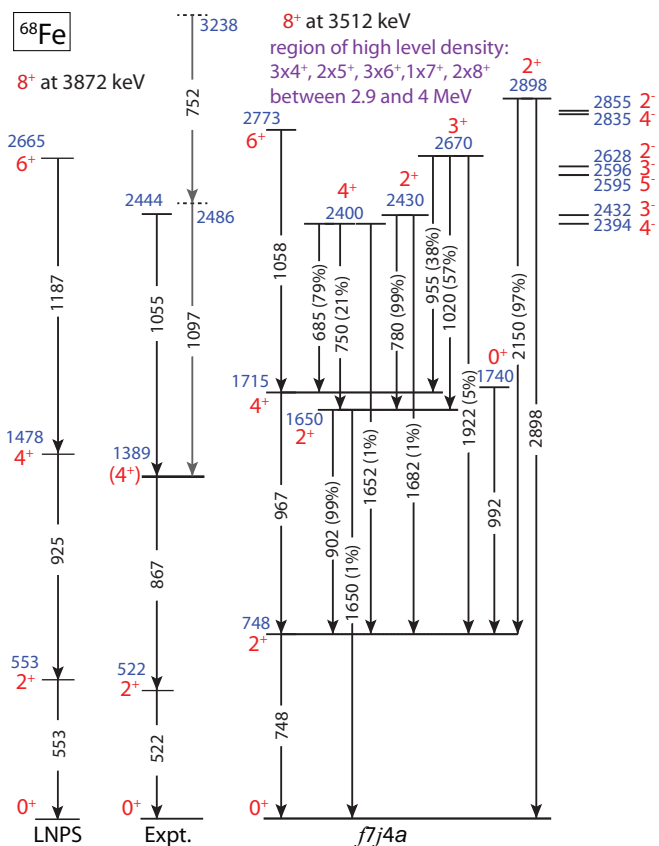

FIG. 6. Calculated yrast level scheme obtained with the LNPS interaction (left) compared to the measurement (middle) and a more extensive level scheme predicted by the $f7j4a$ Hamiltonian (right). For these calculations, one 6^-, 5^-, and 8^- state each, and two 7^- states predicted between 3 and 4 MeV are not shown. The remarkable precision of the LNPS calculations as well as the expected complexity of the level scheme are apparent. From the charge-exchange calculations explained in the text, and from comparisons with the LNPS level scheme, one of the tentative states at around 2.4–2.5 MeV might be viewed as a likely candidate for the 6_1^+ level. For the experimental level scheme, the more precise transition energies of Ref. [11] are used for the decays from the 2_1^+ and (4_1^+) states.

identification of the ^{9}B final states produced by (p, n)-type charge exchange on ^{9}Be, an attempt is presented hereafter to estimate its magnitude together with the expected population pattern of ^{68}Fe excited states. Given that the contribution from multistep reactions at beam energies of ≈ 100 MeV/u is small [36–38], with the possible exception of transitions with a large angular momentum transfer, a direct charge-exchange calculation was carried out leading to a specific final state in ^{9}B. The strong ^{9}Be$_{g.s.}(3/2^-) \rightarrow$ ^{9}B$_{g.s.}(3/2^-)$ transition was chosen, because it carries about $1/3$ of the total Gamow-Teller (GT) strength [39]. Consequently, the cross sections calculated below were multiplied by a factor of 3 to account for contributions from other GT transitions.

Based on Ref. [27], it is assumed that the ^{68}Co projectiles are mostly in the (7^-) ground state, although a ^{82}Se primary beam was employed here instead of ^{76}Ge for which the dominance of ground-state over isomeric content has been

conjectured [27]. The cross section was estimated for the transition from the 7^- ground state to 6^+ final states in ^{68}Fe, assuming a simplified operator $O = [a^\dagger(\nu g_{9/2})a(\pi f_{7/2})]^8$. These calculations were performed with the code FOLD [40], with one-body transition densities (OBTDs) for the ^{9}Be-^{9}B system computed with NUSHELLX@MSU [41]. OBTDs for the $7^- \to 6^+$ excitations in ^{68}Fe were obtained in the normal-modes (NM) formalism with the code NORMOD [42]. The Love-Franey effective NN interaction at 100 MeV [43] was used to create the form factor through a double-folding procedure. The complex optical potentials employed to calculate the ^{9}Be-^{68}Co entrance- and ^{9}B-^{68}Fe exit-channel distorted waves were computed using the methods routinely employed for fast nucleon removal reaction analyses [44].

The calculated total cross section for the $7^- \to 6^+$ excitations below the neutron separation energy with this approach is 0.017 mb; a value much smaller than the measured inclusive one of 0.51(6) mb. However, the calculation only includes transitions to selected final states in ^{9}B and ^{68}Fe. Furthermore, since the momentum transfer is unconstrained in the actual measurement, transitions associated with small and large angular momenta can contribute as well. For spin values between 0 and $8\hbar$, the shell-model calculation predicts the presence of approximately 20 levels below the neutron binding energy of $S_n(^{68}$Fe$) = 5.95$ MeV [45]. Assuming, for simplicity, that the cross sections are proportional to the transition strength for each final-state spin (because of the large angular momentum transfers possible in the reaction) leads to a σ value for the $7^- \to 6^+$ excitations of only about 28% of the total yield. Hence, the inclusive cross section for ^{68}Co$(^9$Be$,^9$B$)^{68}$Fe* charge exchange associated solely with GT transitions in ^{9}B is approximately 0.06 mb.

It is certainly possible that other, non-GT transitions in ^{9}B make up for the additional factor of ≈ 9 necessary to account for the measured inclusive cross section, since the present measurement is final-state inclusive for ^{9}B. Furthermore, only a total of 5% is estimated to feed 0_1^+, 2_1^+, and 4_1^+ states. Hence, these calculations confirm the order of magnitude of the measured inclusive cross section as well as the observed population pattern with little strength to low-lying states. In fact, these results suggest a scenario where high-lying, higher-spin states are populated with their subsequent deexcitations proceeding mostly through lower-spin yrast levels toward the ground state. Admittedly, these schematic calculations are unable to account for the strong direct population of the ground state emerging from the data. A contribution to the cross section from ^{68}Co projectiles in the isomeric 1^+ state would be expected to only account for around 1.0 μb when estimated

from the known B(GT) value of 0.017 derived from β decay [26]. Thus, a full explanation of the reaction mechanism remains a challenge for future studies.

IV. SUMMARY

Excited states in the neutron-rich nucleus ^{68}Fe were populated with a ^{9}Be-induced charge-exchange reaction at 95 MeV/u. The new γ-ray transitions, reported here for the first time, are complementary to the ones observed in β-decay studies and nucleon knockout reactions. Two states at 2.444 and 2.486 MeV are potential candidates for the ^{68}Fe 6_1^+ level, in good agreement with LNPS shell-model calculations. The emerging picture of a reaction with a large cross section, $\sigma_{\text{inc}} = 0.51(6)$ mb, is promising for future in-beam γ-ray spectroscopy studies in view of the observed population pattern where (i) 41% of the direct cross section leads to many high-lying, higher-spin states and (ii) the other 59% feeds the ground state directly. A new, locally optimized Hamiltonian, $f7j4a$, with a model space containing the $0f_{7/2}$ orbital for protons and the $(0f_{5/2}, 1p_{3/2}, 1p_{1/2}, 0g_{9/2})$ ones for neutrons is introduced and employed to provide the nuclear structure input for the simplified charge-exchange reaction calculations. These can account qualitatively for the large cross section and also support observation (i), but fail to explain (ii). While the focus of this work is the use of these reactions as spectroscopic tools, comparisons of ^{12}C- and ^{9}Be-induced charge-exchange reactions may shed light on the interpretation of the reaction mechanism.

[1] F. Nowacki, A. Poves, E. Caurier, and B. Bounthong, Phys. Rev. Lett. **117**, 272501 (2016).

[2] S. M. Lenzi, F. Nowacki, A. Poves, and K. Sieja, Phys. Rev. C **82**, 054301 (2010).

[3] K. Langanke, J. Terasaki, F. Nowacki, D. J. Dean, and W. Nazarewicz, Phys. Rev. C **67**, 044314 (2003).

[4] C. Santamaria, C. Louchart, A. Obertelli, V. Werner, P. Doornenbal, F. Nowacki, G. Authelet, H. Baba, D. Calvet, F. Chateau, A. Corsi, A. Delbart, J.-M. Gheller, A. Gillibert, T. Isobe, V. Lapoux, M. Matsushita, S. Momiyama, T. Motobayashi, M. Niikura *et al.*, Phys. Rev. Lett. **115**, 192501 (2015).

[5] L. Canete, S. Giraud, A. Kankainen, B. Bastin, F. Nowacki, A. Poves, P. Ascher, T. Eronen, V. Alcindor, A. Jokinen, A. Khanam, I. D. Moore, D. A. Nesterenko, F. De Oliveira Santos, H. Penttilä, C. Petrone, I. Pohjalainen, A. de Roubin,

V. A. Rubchenya, M. Vilen, and J. Äystö, Phys. Rev. C **101**, 041304(R) (2020).

[6] F. H. Garcia *et al.*, Phys. Rev. Lett. **125**, 172501 (2020).

[7] M. L. Cortes, W. Rodriguez, P. Doornenbal, A. Obertelli, J. D. Holt, S. M. Lenzi, J. Menendez, F. Nowacki, K. Ogata, A. Poves, T. R. Rodríguez, A. Schwenk, J. Simonis, S. R. Stroberg, K. Yoshida, L. Achouri, H. Baba, F. Browne, D. Calvet, F. Chateau *et al.*, Phys. Lett. B **800**, 135071 (2020).

[8] R. Taniuchi, C. Santamaria, P. Doornenbal, A. Obertelli, K. Yoneda, G. Authelet, H. Baba, D. Calvet, F. Chateau, A. Corsi, A. Delbart, J.-M. Gheller, A. Gillibert, J. D. Holt, T. Isobe, V. Lapoux, M. Matsushita, J. Menendez, S. Momiyama, T. Motobayashi *et al.*, Nature (London) **569**, 53 (2019).

[9] A. Gade, R. V. F. Janssens, D. Weisshaar, B. A. Brown, E. Lunderberg, M. Albers, V. M. Bader, T. Baugher, D. Bazin, J. S. Berryman, C. M. Campbell, M. P. Carpenter, C. J. Chiara, H. L. Crawford, M. Cromaz, U. Garg, C. R. Hoffman, F. G. Kondev, C. Langer, T. Lauritsen *et al.*, Phys. Rev. Lett. **112**, 112503 (2014).

[10] A. Gade, R. V. F. Janssens, J. A. Tostevin, D. Bazin, J. Belarge, P. C. Bender, S. Bottoni, M. P. Carpenter, B. Elman, S. J. Freeman, T. Lauritsen, S. M. Lenzi, B. Longfellow, E. Lunderberg, A. Poves, L. A. Riley, D. K. Sharp, D. Weisshaar, and S. Zhu, Phys. Rev. C **99**, 011301(R) (2019).

[11] J. M. Daugas, I. Matea, J.-P. Delaroche, M. Pfützner, M. Sawicka, F. Becker, G. Bélier, C. R. Bingham, R. Borcea, E. Bouchez, A. Buta, E. Dragulescu, G. Georgiev, J. Giovinazzo, M. Girod, H. Grawe, R. Grzywacz, F. Hammache, M. Ibrahim, M. Lewitowicz *et al.*, Phys. Rev. C **83**, 054312 (2011).

[12] G. Benzoni, A. I. Morales, H. Watanabe, S. Nishimura, L. Coraggio, N. Itaco, A. Gargano, F. Browne, R. Daido, P. Doornenbal, Y. Fang, G. Lorusso, Z. Patel, S. Rice, L. Sinclair, P.-A. Soderstrom, T. Sumikama, J. Wu, Z. Y. Xu, R. Yokoyama *et al.*, Phys. Lett. B **751**, 107 (2015).

[13] S. Suchyta, S. N. Liddick, C. J. Chiara, W. B. Walters, M. P. Carpenter, H. L. Crawford, G. F. Grinyer, G. Gürdal, A. Klose, E. A. McCutchan, J. Pereira, and S. Zhu, Phys. Rev. C **89**, 067303 (2014).

[14] Retrieved from the National Nuclear Data Center (NNDC) ENSDF data base (11/2020).

[15] D. Guillemaud-Mueller, A. C. Mueller, D. Guerreau, F. Pougheon, R. Anne, M. Bernas, J. Galin, J. C. Jacmart, M. Langevin, F. Naulin, E. Quiniou, and C. Detraz, Z. Phys. A **322**, 415 (1985).

[16] M. Bernas, P. Armbruster, S. Czajkowski, H. Faust, J. P. Bocquet, and R. Brissot, Phys. Rev. Lett. **67**, 3661 (1991).

[17] S. Ettenauer, H. Zwahlen, P. Adrich, D. Bazin, C. M. Campbell, J. M. Cook, A. D. Davies, D.-C. Dinca, A. Gade, T. Glasmacher, J.-L. Lecouey, W. F. Mueller, T. Otsuka, R. R. Reynolds, L. A. Riley, J. R. Terry, Y. Utsuno, and K. Yoneda, Phys. Rev. C **78**, 017302 (2008).

[18] S. N. Liddick, B. Abromeit, A. Ayres, A. Bey, C. R. Bingham, B. A. Brown, L. Cartegni, H. L. Crawford, I. G. Darby, R. Grzywacz, S. Ilyushkin, M. Hjorth-Jensen, N. Larson, M. Madurga, D. Miller, S. Padgett, S. V. Paulauskas, M. M. Rajabali, K. Rykaczewski, and S. Suchyta, Phys. Rev. C **87**, 014325 (2013).

[19] M. Hannawald, T. Kautzsch, A. Wöhr, W. B. Walters, K.-L. Kratz, V. N. Fedoseyev, V. I. Mishin, W. Böhmer, B. Pfeiffer, V. Sebastian, Y. Jading, U. Köster, J. Lettry, H. L. Ravn, and the ISOLDE Collaboration, Phys. Rev. Lett. **82**, 1391 (1999).

[20] H. L. Crawford, R. M. Clark, P. Fallon, A. O. Macchiavelli, T. Baugher, D. Bazin, C. W. Beausang, J. S. Berryman, D. L. Bleuel, C. M. Campbell, M. Cromaz, G. de Angelis, A. Gade, R. O. Hughes, I. Y. Lee, S. M. Lenzi, F. Nowacki, S. Paschalis, M. Petri, A. Poves *et al.*, Phys. Rev. Lett. **110**, 242701 (2013).

[21] A. Estrade, M. Matos, H. Schatz, A. M. Amthor, D. Bazin, M. Beard, A. Becerril, E. F. Brown, R. Cyburt, T. Elliot, A. Gade, D. Galaviz, S. George, S. S. Gupta, W. R. Hix, R. Lau, G. Lorusso, P. Moller, J. Pereira, M. Portillo *et al.*, Phys. Rev. Lett. **107**, 172503 (2011).

[22] Z. Meisel, S. George, S. Ahn, D. Bazin, B. A. Brown, J. Browne, J. F. Carpino, H. Chung, R. H. Cyburt, A. Estrade, M. Famiano, A. Gade, C. Langer, M. Matos, W. Mittig, F. Montes, D. J. Morrissey, J. Pereira, H. Schatz, J. Schatz *et al.*, Phys. Rev. C **101**, 052801(R) (2020).

[23] A. Gade, P. Adrich, D. Bazin, B. A. Brown, J. M. Cook, C. Aa. Diget, T. Glasmacher, S. McDaniel, A. Ratkiewicz, K. Siwek, and D. Weisshaar, Phys. Rev. Lett. **102**, 182502 (2009).

[24] A. Lemasson, H. Iwasaki, C. Morse, D. Bazin, T. Baugher, J. S. Berryman, A. Dewald, C. Fransen, A. Gade, S. McDaniel, A. Nichols, A. Ratkiewicz, S. Stroberg, P. Voss, R. Wadsworth, D. Weisshaar, K. Wimmer, and R. Winkler, Phys. Rev. C **85**, 041303(R) (2012).

[25] W. F. Mueller, B. Bruyneel, S. Franchoo, M. Huyse, J. Kurpeta, K. Kruglov, Y. Kudryavtsev, N. V. S. V. Prasad, R. Raabe, I. Reusen, P. Van Duppen, J. Van Roosbroeck, L. Vermeeren, L. Weissman, Z. Janas, M. Karny, T. Kszczot, A. Płochocki, K.-L. Kratz, B. Pfeiffer, H. Grawe *et al.*, Phys. Rev. C **61**, 054308 (2000).

[26] S. N. Liddick, B. Abromeit, A. Ayres, A. Bey, C. R. Bingham, M. Bolla, L. Cartegni, H. L. Crawford, I. G. Darby, R. Grzywacz, S. Ilyushkin, N. Larson, M. Madurga, D. Miller, S. Padgett, S. Paulauskas, M. M. Rajabali, K. Rykaczewski, and S. Suchyta, Phys. Rev. C **85**, 014328 (2012).

[27] C. Izzo, G. Bollen, M. Brodeur, M. Eibach, K. Gulyuz, J. D. Holt, J. M. Kelly, M. Redshaw, R. Ringle, R. Sandler, S. Schwarz, S. R. Stroberg, C. S. Sumithrarachchi, A. A. Valverde, and A. C. C. Villari, Phys. Rev. C **97**, 014309 (2018).

[28] A. Gade and B. M. Sherrill, Phys. Scr. **91**, 053003 (2016).

[29] D. J. Morrissey, B. M. Sherrill, M. Steiner, A. Stolz, and I. Wiedenhöver, Nucl. Instrum. Methods Phys. Res., Sect. B **204**, 90 (2003).

[30] D. Bazin, J. A. Caggiano, B. M. Sherrill, J. Yurkon, and A. Zeller, Nucl. Instrum. Methods Phys. Res., Sect. B **204**, 629 (2003).

[31] A. Gade, R. V. F. Janssens, D. Bazin, P. Farris, A. M. Hill, S. M. Lenzi, J. Li, D. Little, B. Longfellow, F. Nowacki, A. Poves, D. Rhodes, J. A. Tostevin, and D. Weisshaar, Phys. Rev. C **103**, 014314 (2021).

[32] S. Paschalis *et al.*, Nucl. Instrum. Methods Phys. Res., Sect. A **709**, 44 (2013).

[33] D. Weisshaar, D. Bazin, P. C. Bender, C. M. Campbell, F. Recchia, V. Bader, T. Baugher, J. Belarge, M. P. Carpenter, H. L. Crawford, M. Cromaz, B. Elman, P. Fallon, A. Forney, A. Gade, J. Harker, N. Kobayashi, C. Langer, T. Lauritsen, I. Y. Lee *et al.*, Nucl. Instrum. Methods Phys. Res., Sect. A **847**, 187 (2017).

[34] A. F. Lisetskiy, B. A. Brown, M. Horoi, and H. Grawe, Phys. Rev. C **70**, 044314 (2004).

[35] M. Hjorth-Jensen, T. T. S. Kuo, and E. Osnes, Phys. Rep. **261**, 125 (1995); M. Hjorth-Jensen (private communication).

[36] W. von Oertzen, Nucl. Phys. A **482**, 357 (1988).

[37] H. Lenske, H. H. Wolter, and H. G. Bohlen, Phys. Rev. Lett. **62**, 1457 (1989).

[38] S. J. Winfield, N. Anantaraman, Sam M. Austin, L. H. Harwood, J. van der Plicht, H.-L. Wu, and A. F. Zeller, Phys. Rev. C **33**, 1333 (1986).

[39] C. Scholl, Y. Fujita, T. Adachi, P. von Brentano, H. Fujita, M. Górska, H. Hashimoto, K. Hatanaka, H. Matsubara, K. Nakanishi, T. Ohta, Y. Sakemi, Y. Shimbara, Y. Shimizu, Y. Tameshige, A. Tamii, M. Yosoi, and R. G. T. Zegers, Phys. Rev. C **84**, 014308 (2011).

[40] J. Cook and J. Carr, computer program FOLD/DWHI Florida State University (unpublished); based on F. Petrovich and D. Stanley, Nucl. Phys. A **275**, 487 (1977); modified as described in J. Cook, K. W. Kemper, P. V. Drumm, L. K. Fifield, M. A. C.

[41] Hotchkis, T. R. Ophel, and C. L. Woods, Phys. Rev. C **30**, 1538 (1984); R. Zegers, S. Fracasso, and G. Colò (unpublished).

[41] B. A. Brown, W. D. M. Rae, E. McDonald, and M. Horoi, http://www.nscl.msu.edu/~brown/resources/resources.html.

[42] M. A. Hofstee, S. Y. van der Werf, A. M. van den Berg, N. Blasi, J. A. Bordewijk, W. T. A. Borghols, R. De Leo, G. T. Emery, S. Fortier, S. Galès, M. N. Harakeh, P. den Heijer, C. W. de Jager, H. Langevin-Joliot, S. Micheletti, M. Morlet, M. Pignanelli, J. M. Schippers, H. de Vries, A. Willis, and A. van der Woude, Nucl. Phys. A **588**, 729 (1995); S. Y. van der Werf, computer code NORMOD, KVI, University of Groningen, 1991 (unpublished).

[43] M. A. Franey and W. G. Love, Phys. Rev. C **31**, 488 (1985).

[44] J. A. Tostevin and B. A. Brown, Phys. Rev. C **74**, 064604 (2006); J. A. Tostevin (private communication).

[45] W. Meng, G. Audi, F. G. Kondev, W. J. Huang, S. Naimi, and Xu Xing, Chin. Phys. C **41**, 030003 (2017).